Subterahertz monochromatic acoustic wave propagation using semiconductor superlattices as transducers

A. Huynh,[1] B. Perrin,[1] N. D. Lanzillotti-Kimura,[1,2] B. Jusserand,[1] A. Fainstein,[2] and A. Lemaître[3]
[1]*INSP, CNRS, Université Paris 6, 140 rue de Lourmel, 75015 Paris, France*
[2]*Centro Atómico Bariloche and Instituto Balseiro, C. N. E. A., 8400 San Carlos de Bariloche, Argentina*
[3]*LPN, CNRS, Route de Nozay, 91460 Marcoussis, France*
(Received 25 July 2008; published 4 December 2008)

We demonstrate both semiconductor superlattices and nanocavities as narrow-band acoustic transducers in the subterahertz range. Picosecond ultrasonics with pump and probe incident on opposite sides of the substrate allows full decoupling of the phonon generation and detection processes. Pumping in the nanotransducers, we generate spectrally narrow wave packets which propagate over macroscopic distances. Probing in the nanotransducers, we evidence them as very sensitive and spectrally selective detectors.

DOI: 10.1103/PhysRevB.78.233302 PACS number(s): 78.47.−p, 43.38.+n, 63.20.−e

A typical pulse echo experiment works with emitter and detector of acoustic waves pulses, deposited on opposite sides of a macroscopic sample. Piezoelectric transduction is very efficient up to a few gigahertz but only special geometries can work beyond 100 GHz.[1] The goal of this Brief Report is to show that optical transduction with semiconductor superlattices (SLs) can be used according the same lines but with a frequency range extending up to 1 THz. The availability of efficient monochromatic phonons transducers in the terahertz range would give access to studies of vibrational properties in amorphous and quasicrystalline materials, in nanostructures, or in any system exhibiting inhomogeneities at the nanometer scale. These waves could also be used for high-resolution acoustic microscopy and to drive the optical and electronic properties of devices at the picosecond time scale. Propagation of terahertz phonons by heat-pulse techniques has been extensively studied since the pioneering work of von Gutfeld[2] but these phonons are incoherent and very broadband. Tunneling junctions[3,4] provide monochromatic but still incoherent sources. Later, coherent acoustic wave generation and detection by an optical pump-probe technique and a femtosecond laser source proved to be very successful.[5] Using a metallic film as a transducer, generation and detection of very short acoustic pulses with a broad frequency spectrum extending up to a few hundreds of gigahertz can be performed. Quantum well (QW) transducers have been also introduced.[6] However they remain broadband transducers with a high-frequency cutoff limited by the QW thickness. Regularly stacking several QWs and then building superlattices should result in an enhancement of the transduction efficiency. More important, SLs offer a unique access to high-frequency monochromatic acoustic phonon optical transduction. High-frequency folded modes are strongly coupled to light in SL and the terahertz range can be reached with typical periods of a few nanometers, easily controlled by modern deposition techniques. Moreover, the periodic modulation of the elastic properties leads to the opening of energy gaps in the Brillouin-zone center and boundary. Light scattering has provided a detailed understanding of the SL vibrations at thermal equilibrium,[7] while ultrafast optics experiments also showed that high-frequency modes can be coherently excited and controlled.[8–13] The initial proposal of SL as potentially ideal monochromatic optical transducers for coherent phonons[14] has however received up to now very limited experimental demonstration. Propagation through a substrate of acoustic pulses optically excited in SLs was first reported using an incoherent detection with a superconducting bolometer deposited on the other side of the sample.[15] A subsequent experiment using a second SL as an acoustic filter gave support to the coherence of the emitted phonons,[16] though leaving the spectral width of the generated phonons unknown.

In this work we give direct evidence of the transduction of coherent monochromatic longitudinal-acoustic phonons using SL or recently introduced acoustic nanocavities,[17,18] by detecting these phonons with a pump-probe technique after they propagate through a thick substrate. Indeed, in contrast with classical pump and probe experiments where both generation and detection are performed on the device surface, here the generation process takes place in the device, whereas the detection is done on the backside with a broadband metallic transducer. The generated phonons then cannot be described as a broadband pulse with a duration in the picosecond range but as quasimonochromatic coherent oscillations with duration in the nanosecond range. Alternatively, the metallic layer is also used as a coherent broadband generator to demonstrate that SLs are very sensitive and frequency-selective phonon detectors. In these experiments, the propagation of the generated acoustic signal over a large distance allows the decoupling of generation and detection processes. Moreover, during propagation, nonlinear distortion of the initial acoustic signal is likely to occur at high displacement amplitudes, which could give rise to acoustic solitons[19,20] and high-frequency conversion. Sound attenuation is made negligible across the thick GaAs substrate (330–380 μm) by cooling down samples to 15 K. Finally we compare the transduction performances of the standard SL and the nanocavity devices. We show that the latter provides an unsurpassed ultimate linewidth associated with confined undispersive cavity phonons, while the overall behaviors of the two devices remain qualitatively similar.

Owing to the limitations of the aluminum transducer, we choose to work on semiconductor structures grown on double side–polished [001] GaAs substrate, with a zone-

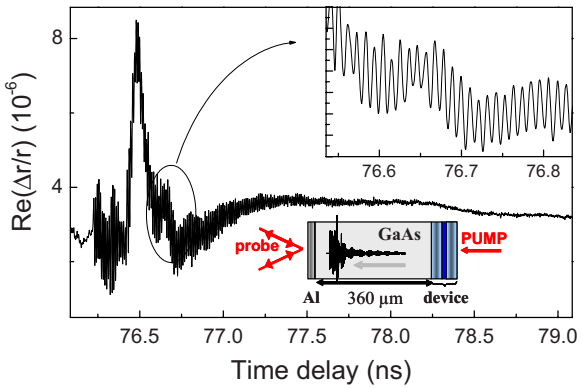

FIG. 1. (Color online) $\mathrm{Re}(\Delta r/r)$ on sample M1 as a function of the pump-probe delay. The insets show an expanded region and a scheme of the picosecond ultrasonics measurement (configuration 1), where a calculated temporal trace of the strain generated by the device is drawn.

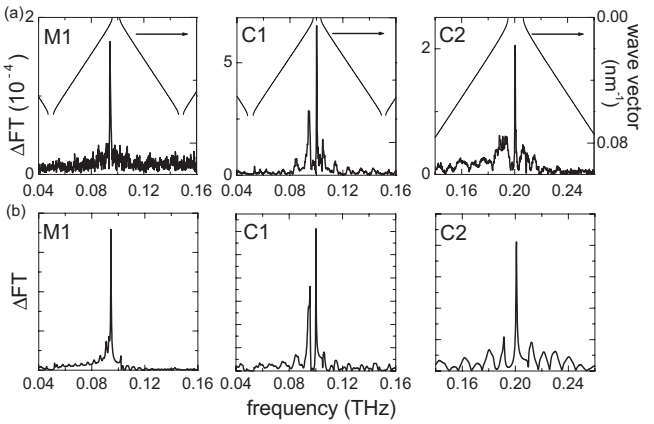

FIG. 2. Configuration 1. (a) Fourier-transform amplitudes of the time derivative of $\mathrm{Im}(\Delta r/r)$, compared to the folded phonon dispersion. The pump power is 5 nJ/pulse. (b) Corresponding calculations.

center first gap located at 100 or 200 GHz. The first ones contain 35 nm/15 nm GaAs/AlAs SL, resulting in opening gaps every 50 GHz, whereas for 200 GHz SL, layers are twice thinner and gaps open every 100 GHz. Sample M1 (M2) is a 20-period (40-period) SL designed at 100 GHz (200 GHz). With SL acting as an acoustic Bragg mirror, surface-localized modes can be confined in superficial layers of the mirror since the interface with air is a perfect reflector[8,10] but an acoustic nanocavity can also be obtained if a GaAs layer is sandwiched between two such mirrors. We present results on cavities containing ten-period Bragg mirrors: sample C1 (C2) with an acoustic confined mode at 100 GHz (200 GHz) and a cavity thickness of 23 nm (37 nm). For all samples, the light absorption threshold is about 810 nm at low temperature.

When a laser pump beam interacts with such nanostructures, an acoustic strain modulated at the superlattice period is created, and generation of very-high-frequency coherent phonons is expected in a narrow frequency range. To demonstrate this generation, we performed a first set of experiments (named afterward as configuration 1; cf. inset of Fig. 1) where the pump pulse is focused directly on the device, generating acoustic phonons which propagate through the whole substrate. They are detected by a time-delayed probe pulse reflected by a 30-nm-thick Al layer deposited on the other side of the sample.

We used a femtosecond mode-locked Ti:sapphire laser providing 130 fs pulses at 750 nm, with an 80 MHz repetition rate. At this wavelength, the absorption length in the device, $1/\alpha$, is comparable to the multilayer thickness. The transient changes of the complex optical reflectivity $\Delta r/r$ are measured by a Sagnac interferometer.[21] The pump is modulated at 1 MHz and the probe is detected by a lock-in amplifier. Both beams are focused onto 60 μm spots with a typical energy of a few nanojoules per pulse for the pump.

A typical signal (obtained on sample M1) corresponding to the real part of $\Delta r/r$ is shown in Fig. 1. Due to the very thick substrate, no direct electronic or thermal contributions appear except a standard acoustic pulse. Its width amounts to 140 ps, in good agreement with the expected value of αv^{-1}, where v is the averaged velocity in the device (5 nm/ps). The maximum of the signal gives the arrival time of the acoustic pulse (76.5 ns) taking into account acoustic reflections on the free surfaces of both Al film and device. Moreover, high-frequency oscillations extending over a few nanoseconds with an amplitude of 10^{-6} are clearly visible. They start 200 ps before the signal maximum, a delay corresponding to the transit time through the device. The first oscillations are due to the acoustic signal generated by the device's deepest layers, i.e., the last ones before the substrate. Figure 2(a) shows the Fourier-transform amplitude of the time derivative (ΔFT) of the signals over a 3 ns time window to ensure a sufficient frequency resolution (0.3 GHz). Note that both real and imaginary parts of $\Delta r/r$ give similar spectral information. The acoustic resonances of a mirror made of m periods d occur at energies corresponding to wave vectors $q=n\pi/md$, with $n \in \mathbb{N}$ but $\frac{n}{m} \notin \mathbb{N}$ in the extended Brillouin zone of the related infinite structure. Moreover, for a weakly absorbing structure, an enhancement of the generation process is mostly expected near the zone center of the reduced Brillouin zone. Thus the lowest-energy large peaks in the Fourier spectrum are expected at $qd=2\pi \pm \pi/m$, among smaller resonances. From symmetry considerations applied to the lowest zone-center gap, only the mode below lower gap edge should be excited in our structures. It will be referred to the forward-scattering (FS) mode as the same mode is Raman active in forward-scattering configuration. The comparison of the experimental spectra with the dispersion curve [see Fig. 2(a)] shows that the excited peak corresponds to this mode. As $m=20$, it is indeed slightly downshifted relatively to $q=0$ mode. In sample C1, the FS mode can also be observed, but at a larger distance from the zone center since acoustic mirrors of the cavity have only $m=10$ periods. The most remarkable fact, however, is the presence of a very narrow cavity mode in the middle of the first zone-center gap.

To analyze these results, we perform calculations of the acoustic field in the multilayers with a standard transfer-matrix formalism.[22] We calculate the electromagnetic field in each layer and assume that the interaction of the device with the incoming light leaves a stress proportional to the local

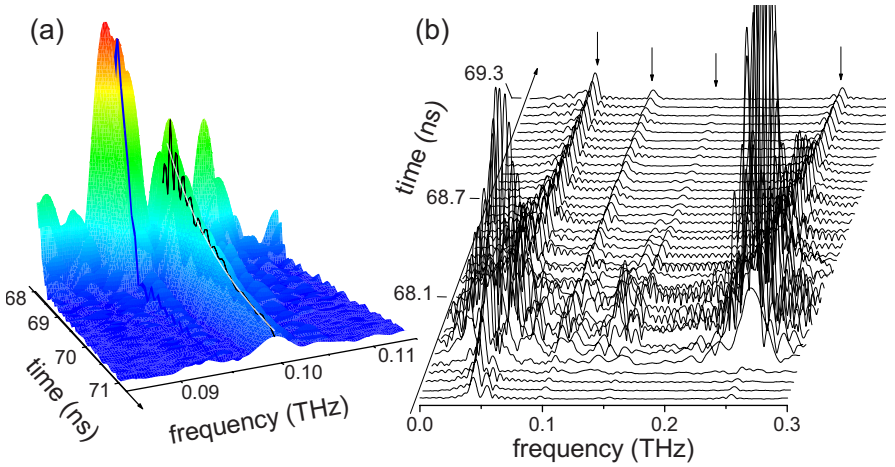

FIG. 3. (Color online) Sliding Fourier transforms of the time derivatives of (a) $\mathrm{Im}(\Delta r/r)$ and (b) $\mathrm{Re}(\Delta r/r)$ for sample C1. The time indicates the center of the Fourier-transform window. (a) Configuration 1. The line at 95 GHz (the black line at 100 GHz) follows the decay of the lower band-edge peak (the cavity mode). The white line is an exponential fit. (b) Configuration 2. Arrows show the cavity modes at 0.05, 0.15, and 0.25 THz for zone boundaries and 0.1 THz for the zone center.

electromagnetic field energy in GaAs layers only. The sound wave propagation equation is solved in each layer, taking into account this stress source term and boundary conditions to obtain the acoustic field everywhere. We measure in $\Delta r/r$ 100 GHz oscillations of 10^{-6}, and the strain incident on the Al film at this frequency is estimated to be $\sim 10^{-6}$. At such strain, nonlinear effects are negligible. We then calculate the imaginary part of $\Delta r/r$ [Fig. 2(b)], including contributions of the surface displacement and photoelastic effects in aluminum, in excellent agreement with the experimental data. The same conclusion applies at higher frequencies for sample C2 emitting at 200 GHz (Fig. 2).

The cavity mode width deduced for C1 from a 3 ns time integration is $\Delta f = 0.5$ GHz to be compared with the theoretical limit of 0.32 GHz given by the quality factor. Another way to analyze the lifetime of the generated phonon modes is to perform sliding Fourier transform over 300 ps time windows whose central value scans the whole time range. Results are reported in Fig. 3(a) for sample C1: the cavity mode lives much longer than the acoustic mirror resonances as this mode tunnels slowly outside the cavity owing to the confinement. We can deduce an exponential decay of 1300 ± 200 ps, in agreement with the measured linewidth $\sqrt{3}/(\pi \Delta f)$ (1100 ps).

To summarize we have demonstrated in the first part that SLs and cavities efficiently generate monochromatic phonons which escape from the device and propagate through a thick substrate before being detected on the other side via a metallic transducer. Let us now consider the detection performance of these nanostructures. In a semitransparent material, the interaction of light with coherent phonons is strongly enhanced at a particular acoustic wave vector $q = 2k$, where k is the electromagnetic wave vector in the sample.[5] The same modes are Raman active in backscattering configuration. At the experimental wavelength, q is close to the zone edge in samples M1 and C1, and in the middle of the Brillouin zone in samples M2 and C2. The Brillouin mode corresponds to the lowest frequency. This enhanced detection has been demonstrated in the second set of experiments where the pump beam is absorbed in the Al layer, generating a broadband acoustic pulse due to the short optical absorption length. In this case, propagation through the whole substrate strongly modifies the spectrum of the pulse and high-frequency conversion is expected (configuration 2; see inset of Fig. 4, where the strain generated by the Al film and the same strain after nonlinear propagation are schematically shown). The detection of the resulting acoustic pulse by the device on the other side allows one to study the detection process without mixing with the generation mechanism, and to take advantage of nonlinear frequency conversion to test the detector sensitivity at high frequencies.

Figure 4(a) shows the real part of $\Delta r/r$ obtained on sample M2. The Brillouin oscillations can be observed on the whole time window, whereas superimposed high-frequency features occur during the round trip duration of the acoustic pulse in the multilayer, indicated by the arrows. Indeed, the probe beam is not fully absorbed in the device and interacts in the substrate with the incoming acoustic pulse before it reaches the device, or when it leaves the device, after reflection on the free surface. Figure 4(b) shows the ΔFT of this temporal trace. As expected, few discrete frequencies corresponding to the enhanced detection selection rule are ob-

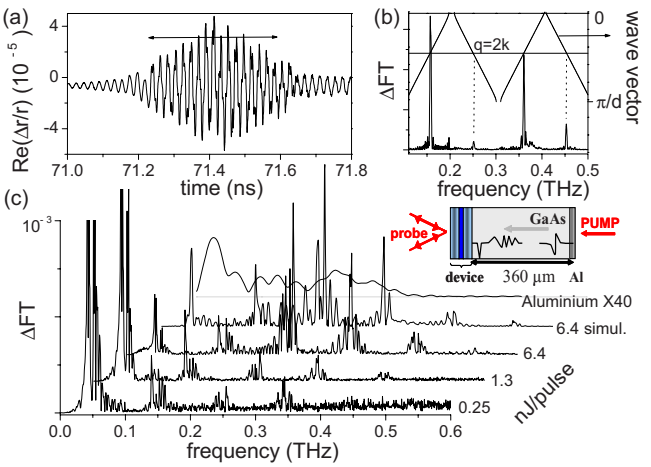

FIG. 4. (Color online) Inset: Scheme of the experimental configuration 2. (a) $\mathrm{Re}(\Delta r/r)$ as a function of the pump-probe delay on sample M2 (arrows indicate the acoustic pulse round trip in the device). (b) Corresponding spectra, compared with the folded dispersion. (c) Amplitudes of the time derivative of $\mathrm{Re}(\Delta r/r)$, normalized to 1 nJ/pulse, measured (i) on sample M1 at different pump intensities compared to a calculation for 6.4 nJ/pulse and (ii) on a sample where the detector is an Al film at 7.6 nJ/pulse.

served among Bragg oscillations due to device finite size. We show in Fig. 3(b) sliding ΔFT calculated over 200 ps time window for sample C1. As already mentioned, detection is enhanced close to the zone edge in this structure and the lowest folded mode almost coincides with the Brillouin oscillation. The Brillouin mode is detected first, while folded modes are only observed during the time they remain in the device. Moreover, we see the long-lived cavity modes within the zone-boundary acoustic gaps (50 and 150 GHz) and the zone-center one at 100 GHz (at 200 GHz the gap is closed). This demonstrates that cavity modes can be excited just hitting the device with an acoustic pulse. In contrast to the mirror modes, they can be still detected after 68.5 ns during the long time they take to leave the cavity, which is much greater than 430 ps, time corresponding to the round trip in the device.

Let us now consider the effect of high-frequency transfer during the nonlinear propagation in the GaAs substrate. Figure 4(c) shows the ΔFT of $\mathrm{Re}(\Delta r/r)$ normalized by the pump pulse energy measured in sample M1 with different energies from 0.2 to 6.4 nJ. As in C1, the signal is large around the zone-boundary gaps. On the curve obtained with a low-intensity pump (0.25 nJ/pulse), the frequency range detected in M1 extends to 350 GHz, and up to 550 GHz for the largest intensity. Distortion during propagation through the substrate due to sound dispersion and nonlinear effects can be described by a one-dimensional (1D) Korteweg–de Vries equation[19,23] as far as diffraction is negligible. Sound absorption is negligible at low temperature. Solving this equation, the spectrum of the acoustic pulse incident on the device has been calculated and $\mathrm{Re}(\Delta r/r)$ of the device obtained with a standard method[22,24] is shown in Fig. 4(c) for 6.4 nJ/pulse pump intensity. The incoming strain on the device can be estimated to be 6×10^{-4}. In similar experiments performed with an aluminum detector;[20] i.e., on a GaAs substrate with aluminum on both sides, frequencies of up to 200 GHz have been observed with a low-power excitation and up to 350 GHz for 7.6 nJ/pulse as illustrated in Fig. 4(c). Moreover, the detected signal was more than 1 order of magnitude weaker. These results demonstrate that semiconductor multilayers are in comparison very efficient detectors at high frequencies.

In summary, we have introduced an experimental scheme combining a white acoustic transducer (Al film) and a quasimonochromatic one (semiconductor multilayer). This allowed us to perform two sets of experiments which demonstrate independently that phonon mirrors and acoustic cavities are efficient quasimonochromatic phonon generators and also selective and sensitive phonon detectors. We show that standard models provide a reasonable understanding of our results. Nevertheless, these experimental configurations will allow future detailed studies of generation and detection mechanisms. As the Al film and the multilayer are deposited on the opposite sides of a thick substrate, in contrast with experiments performed in front configuration, we clearly show that coherent phonons generated in the device can be efficiently transferred into the substrate where they can propagate over millimetric distances. This transduction efficiency should work in the terahertz range provided that two such devices are used for the generation and detection. This would allow phonon imaging and spectroscopy in nanostructures using acoustic waves with nanometric wavelengths.

[1] J. Ilukor and E. H. Jacobsen, *Physical Acoustics* (Academic, New York, 1968), Vol. V, p. 221.
[2] R. J. von Gutfeld and A. H. Nethercot, Jr., Phys. Rev. Lett. **12**, 641 (1964).
[3] W. Eisenmenger and A. H. Dayem, Phys. Rev. Lett. **18**, 125 (1967).
[4] H. Kinder, Phys. Rev. Lett. **28**, 1564 (1972).
[5] C. Thomsen, H. T. Grahn, H. J. Maris, and J. Tauc, Phys. Rev. B **34**, 4129 (1986).
[6] O. Matsuda, T. Tachizaki, T. Fukui, J. J. Baumberg, and O. B. Wright, Phys. Rev. B **71**, 115330 (2005).
[7] B. Jusserand and M. Cardona, *Light Scattering in Solids V* (Springer, Heidelberg, 1989), p. 49.
[8] H. T. Grahn, H. J. Maris, J. Tauc, and B. Abeles, Phys. Rev. B **38**, 6066 (1988).
[9] W. Chen, Y. Lu, H. J. Maris, and G. Xiao, Phys. Rev. B **50**, 14506 (1994).
[10] B. Perrin, B. Bonello, J.-C. Jeannet, and E. Romatet, Physica B **219–220**, 681 (1996).
[11] K. Mizoguchi, M. Hase, S. Nakashima, and M. Nakayama, Phys. Rev. B **60**, 8262 (1999).
[12] N.-W. Pu, Phys. Rev. B **72**, 115428 (2005).
[13] A. Bartels, T. Dekorsy, H. Kurz, and K. Köhler, Phys. Rev. Lett. **82**, 1044 (1999).
[14] P. Basséras, S. M. Gracewski, G. W. Wicks, and R. J. D. Miller, J. Appl. Phys. **75**, 2761 (1994).
[15] P. Hawker, A. J. Kent, L. J. Challis, A. Bartels, T. Dekorsy, and H. Kurz, Appl. Phys. Lett. **77**, 3209 (2000).
[16] N. M. Stanton, R. N. Kini, A. J. Kent, M. Henini, and D. Lehmann, Phys. Rev. B **68**, 113302 (2003).
[17] M. Trigo, A. Bruchhausen, A. Fainstein, B. Jusserand, and V. Thierry-Mieg, Phys. Rev. Lett. **89**, 227402 (2002).
[18] A. Huynh, N. D. Lanzillotti-Kimura, B. Jusserand, B. Perrin, A. Fainstein, M. F. Pascual-Winter, E. Peronne, and A. Lemaître, Phys. Rev. Lett. **97**, 115502 (2006).
[19] H.-Y. Hao and H. J. Maris, Phys. Rev. B **64**, 064302 (2001).
[20] E. Peronne and B. Perrin, Ultrasonics **44**, e1203 (2006).
[21] J.-Y. Duquesne and B. Perrin, Phys. Rev. B **68**, 134205 (2003).
[22] C. Rossignol and B. Perrin, Anal. Sci. **17**, 245 (2001).
[23] O. L. Muskens, A. V. Akimov, and J. I. Dijkhuis, Phys. Rev. Lett. **92**, 035503 (2004).
[24] B. Perrin, Prog. Nat. Sci. **6**, 444 (1996).